Journal of Alloys and Compounds 950 (2023) 169891

Contents lists available at ScienceDirect

Journal of Alloys and Compounds

journal homepage: www.elsevier.com/locate/jalcom

Structure and dielectric properties of yttrium-doped $Ca_{0.28}Ba_{0.72}Nb_2O_6$ ceramics

Harry Peirson [a,*], Juncheng Pan [b], Yizhe Li [b], David A. Hall [b], Andy P. Brown [a], Rik M. Drummond-Brydson [a], Steven J. Milne [a]

[a] School of Chemical and Process Engineering, University of Leeds, Leeds LS2 9JT, UK
[b] Department of Materials, University of Manchester, Oxford Road, Manchester M13 9PL, UK

ARTICLE INFO

Article history:
Received 23 December 2022
Received in revised form 27 March 2023
Accepted 29 March 2023
Available online 30 March 2023

Keywords:
Ceramics
Ferroelectrics
Dielectric response
Tungsten-bronze

ABSTRACT

An unfilled tungsten bronze-structured ferroelectric ceramic, $Ca_{0.28}Ba_{0.72}Nb_2O_6$ (CBN28), has been doped with Y^{3+} to produce ceramics with a nominal composition, $(Ca_{0.28}Ba_{0.72})_{1-3w/2}Y_wNb_2O_6$ [$0 \le w \le 0.05$]. The substitution of Y^{3+} for Ca^{2+}/Ba^{2+}, and consequent additional vacancy formation, is assumed to occur on the A1/A2 sites. This resulted in a minor reduction of the c lattice parameter, and unit cell volume. For undoped CBN28, there was a slightly diffuse relative permittivity-temperature (ε_r-T) peak at 268 °C. The peak became much broader for sample compositions w = 0.04 and 0.05 and the peak temperature showed a level of frequency dependence consistent with weak relaxor behaviour. The polarisation-electric field loops became narrower for samples w = 0.04 and 0.05, corresponding to a reduction in remnant polarisation value, from 2.4 to 0.8 μC cm^{-2} (30 kV cm^{-1}). The Y doped ceramics exhibited stable relative permittivity over a wide temperature range, the variation being within ± 15% of the median value from 36 °C to 218 °C for w = 0.05, when measured at 1 kHz. Consequently, we suggest that A site donor-doping and aliovalent B site doping of CBN holds potential for industry standard, temperature stable, high temperature dielectrics ($\varepsilon_r \ge 500$ ± 15% from - 55–250 + °C).

1. Introduction

Tungsten bronze-structured niobate ceramics have received attention due to promising ferroelectric and optical properties [1,2]. More recent work has demonstrated a tungsten bronze (TB) structured ceramic with near temperature stable dielectric permittivity from − 55–300 °C by doping strontium sodium niobate (SNN) with Y, Zr and Ca [3].

Structurally, tungsten bronzes consist of a matrix of corner sharing (BO_6) oxygen octahedra of two orientations ($B1O_6$ and $B2O_6$) tilted in such a way to create three different sites for occupancy by other cations, the general formula being $(A2)_4(A1)_2(C)(B1)_2(B2)_8O_{30}$. These three sites (A2, A1 and C), have coordination numbers of 15, 12 and 9 respectively and represent pentagonal, square, and triangular channels along the *c*-axis of the unit cell, Fig. 1. The origins of a spontaneous polarisation in tungsten bronzes (TBs) are more complex than for perovskite ferroelectrics. For niobate TBs, displacement of Nb^{5+} within the NbO_6 octahedra occurs primarily along the c-axis. The $B2O_6$ octahedra may also tilt out of plane, disrupting these ordered NbO_6 chains [4]. In CBN, this octahedral tilting and rotation can give rise to commensurate or incommensurate modulation [5,6].

Tungsten bronzes may be classed as 'filled' or 'partially filled/unfilled' depending on full or partial occupancy of the A2 and A1 sites. The much smaller C sites are usually empty, but the term 'stuffed' is applied should they be occupied (by Li^+ for example). Calcium barium niobate (CBN) solid solutions are examples of 'unfilled' TBs as only five of the available six A2/A1 sites are occupied in the formula $(Ca_x Ba_{1-x})_5Nb_{10}O_{30}$, more commonly written $(Ca_xBa_{1-x})Nb_2O_6$.

For single crystal $Ca_{0.28}Ba_{0.72}Nb_2O_6$ (CBN28), Graetsch et al. refined the X-ray diffraction data to space group P4bm [7]. They reported that an incommensurate modulation originates from the distribution of Ca, Ba and vacancies on the 15 co-ordinate A2 sites [7]. This induces a displacive modulation of the adjacent O atoms with amplitudes up to 0.2 Å, which results in NbO_6 octahedra being cooperatively tilted from their average positions [7]. High resolution transmission electron microscopy and electron diffraction studies provided direct evidence of the incommensurate modulation of CBN28 superstructure [6]. The A2 sites were found to be occupied predominantly by Ba^{2+}, whilst Ca^{2+} was the dominant occupant of the smaller 12 co-ordinate A1 sites. However, there was a minor level of mixed site occupancy by Ba^{2+} and Ca^{2+} [7]. Previously it had

* Corresponding authors.
E-mail address: pm14hjp@leeds.ac.uk (H. Peirson).

https://doi.org/10.1016/j.jallcom.2023.169891

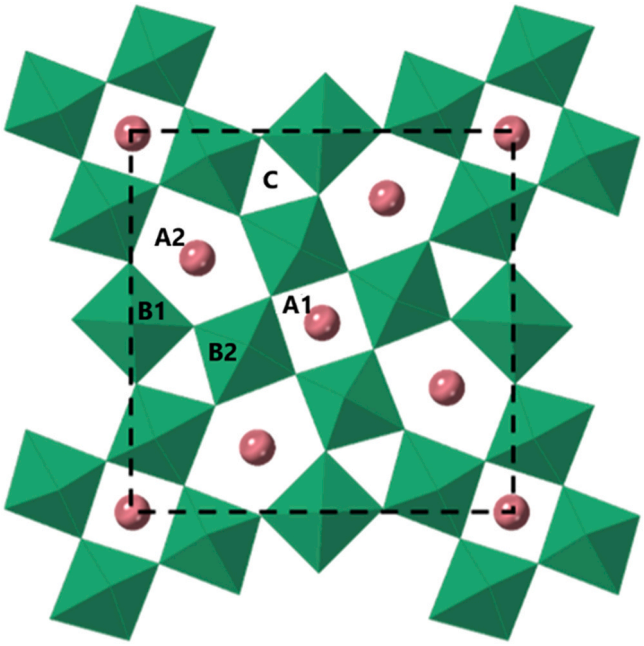

Fig. 1. The tetragonal tungsten bronze structure, $(A2)_4(A1)_2(C)\,(B1)_2(B2)_8O_{30}$, viewed along the [001], with tetragonal unit cell projections marked out (dotted lines). Interstitial sites A1, A2 and C exist within a matrix of corner-sharing NbO_6 octahedra of varying tilt.

been suggested that the smaller Ca^{2+} ion occupied the 12 co-ordinate A1 sites exclusively, with Ba^{2+} only located on the larger 15 co-ordinate A2 sites [8].

In the ferroelectric phase, both types of symmetrically non-equivalent NbO_6 octahedra (B1 and B2) are distorted by displacement of the Nb atoms along the tetragonal c-axis [9] On heating above room-temperature, the Nb displacements gradually decrease [9]. However, some structural distortions were reported to persist above the temperature of the peak in relative permittivity and result in fluctuating polar nanodomains [9]. The dynamics of polar nanoregions and the extent of relaxor behaviour was found to vary with increasing Ca/Ba ratio (x) for the $Ca_xBa_{1-x}Nb_2O_6$ solid solution series, $0.18 \le x \le 0.35$ [10]. The x = 0.28 composition corresponds to 'CBN28′, studied in the present work.

We selected CBN28 as a promising material in the context of developing temperature-stable Class II dielectrics. These should show a variation in relative permittivity, ε_r, of no more than ± 15% across wide temperature ranges, ideally from − 55–250 °C or 300 °C, with minimum ε_r values > 500. Commercial Class II capacitors are generally based on ferroelectric $BaTiO_3$ as the dielectric. Dopants and microstructural strain produce a smeared out or flattened ε_r-T response facilitating a consistent permittivity from − 55–125 °C in the so called X7R commercial formulations. However, because the Curie point (ε_r -T peak temperature) of $BaTiO_3$ is only ~130 °C, substitutionally modified $BaTiO_3$ cannot retain high permittivity to temperatures of 200–300 °C, as required of new capacitor materials for modern power electronics applications. The relatively high temperature of the ε_r -T peak for CBN28, ~ 270 °C, as opposed to ~130 °C for $BaTiO_3$, makes CBN28 a promising starting point in the context of devising new higher temperature dielectrics through compositional engineering.

There are a number of Pb or Bi containing perovskite-structured dielectrics that go some way to satisfying the new requirements for operation above 200 °C [11–14]**.** However, the oxides of both Pb and Bi are thermodynamically incompatible with the manufacture of nickel base metal electrode multilayer ceramic capacitors, the main market sector. Moreover, Pb is toxic.

Recently a material based on the formulation $Sr_2NaNb_5O_{15}$ was demonstrated by our laboratory to result in a ceramic with ε_r > 1000 and better that 15% stability from − 55 °C to ~300 °C [3]. But it presents significant drawbacks in terms of capacitor applications. The product which results from sintering (1300 −1400 °C) and normal furnace cooling procedures is a two-phase mixture of a tungsten bronze solid solution of $Sr_{2+x}Na_{1-2x}Nb_5O_{15}$ (SNN) phase with x ~ 0.05 and a perovskite phase $Na_{1-2x}Sr_xNbO_3$ [15]. Although SNN can be produced as a single phase for compositions $0.05 \le x \le 0.2$, charge-balancing Na ion vacancies increase with increasing x values, which is undesirable for capacitor applications.

Any soda loss which occurs by volatilisation during calcination and sintering would increase the concentration of sodium vacancy defects and also create oxygen vacancies, adding to the likelihood of electrical conductivity and low dielectric strength problems. There is a further, fundamental obstacle to SNN: it is metastable below ~1200 °C [15] although the rate of decomposition at temperatures of relevance to capacitors has yet to be established.

These problems facing Pb, Bi or Na containing high temperature ceramic dielectrics motivated us to consider alternative ceramic systems. Here, we investigate the properties of $Ca_{0.28}Ba_{0.72}Nb_2O_6$ ceramics modified by Y^{3+} 'donor' substitution and examine dielectric and ferroelectric properties.

2. Experimental

Ceramics of formulation $(Ca_{0.28}Ba_{0.72})_{1-3w/2}Y_wNb_2O_6$ [$0 \le w \le 0.05$] were produced by the conventional mixed oxide process with the assumption that the Y^{3+} substituent will occupy A1/A2 sites. Appropriate quantities of the following oxides and carbonates were dried at 200 °C for at least 24 h and ball milled with yttria stabilised zirconia milling media and isopropanol for 24 h: $CaCO_3$ (Alfa Aesar, 99.95%); $BaCO_3$ (Alfa Aesar, 99.95%); Nb_2O_5 (Alfa Aesar, 99.9%); Y_2O_3 (Alfa Aesar, 99.9%).

Dried, milled powders were calcined at 1200 °C for 4 h in covered alumina crucibles (heating rate 5 °C/min). Calcined powders were sieved through 300 µm nylon mesh and milled again with 2 wt% binder (Opitax AC112, Zschimmer & Schwarz) before drying, sieving, and pressing uniaxially at 180 MPa for 30 s in a 10 mm diameter steel die. Green pellets were then heated at 550 °C for 5 h to promote binder burn-out (heating rate 1 °C/min). To obtain high relative densities (≥ 94%), a two-stage sintering regime was employed (heating and cooling rate 5 °C/min). The undoped $Ca_{0.28}Ba_{0.72}Nb_2O_6$ and doped $(Ca_{0.28}Ba_{0.72})_{1-3w/2}Y_wNb_2O_6$ [w = 0.02] formulations were heated to 1350 °C and then immediately cooled to 1200 °C for a dwell time of 4 h. The $(Ca_{0.28}Ba_{0.72})_{1-3w/2}Y_wNb_2O_6$ [w = 0.04 and w = 0.05] formulations were heated to 1325 °C then cooled to 1250 °C for a dwell time of 4 h.

X-ray powder diffraction (XRD) was performed on crushed sintered pellets by rotating the samples in a Bruker D8 powder diffractometer (Bruker, Germany), using Cu Kα X-ray radiation (wavelength 1.5406 Å) for 12 h scans measured from 10 to 90 °2θ, with a step size of 0.008 °2θ and a time per step of 4.2 s. Unit cell lattice parameters for the Pb4m phase of CBN were obtained by full pattern Rietveld refinement using TOPAS 5.0 software (Bruker AXS, Karlsruhe, Germany). In the refinement analysis, the peak shape function was determined by the X-ray diffractometer geometry, and fundamental background parameters. Lattice constants, scale factor, atomic coordination and occupancy were refined. Maximum theoretical densities were calculated from unit cell atomic masses and lattice parameters obtained from the refinement outlined above. Measured ceramic densities were calculated via the geometric method.

Sintered ceramic pellets were mounted in epoxy resin (Epothin, Buehler), in preparation for microstructural examination. These samples were ground with silicon carbide abrasive paper (P800 and

P2500) and polished using Texmet P microcloths then MetaDi 2 diamond suspensions with sequentially decreasing particle sizes of 9, 3 and 1 µm (Buehler, Germany). Chemical etching was carried out at room temperature with a 2:1 ratio of hydrofluoric acid and concentrated nitric acid for 180 s. Scanning electron microscopy was undertaken on sample pellets sputter coated with 20 nm amorphous carbon, in a Hitachi SU8230 high performance, cold field emission instrument operating at 2 kV and 5000x magnification.

For electrical measurements, silver electrodes (Gwent Electronic Materials) were deposited on ceramic pellets at a firing temperature of 550 ºC for 5 h. Relative permittivity and dielectric loss were measured as a function of temperature by using a HP4284a LCR analyser (Hewlett Packard, USA); frequencies ranged from 10^3-10^6 Hz and temperatures from 20 to 350 ºC. A controlled environment chamber was used for lower temperatures down to − 70 ºC (Tenney Environmental-SPX, White Deer).

Ferroelectric hysteresis measurements were performed by applying four sinusoidal cycles of an AC electric field waveform with a frequency of 2 Hz, using a function generator (HP33120A, Keysight Technologies, Berkshire, UK) and a high voltage amplifier (HVA1B, Chevin Research, Otley, UK). The electric field was calculated directly from the recorded voltage waveform, while the corresponding polarisation values were obtained by integration of the current with respect to time using LabVIEW software [16]. Polarisation-electric field (P-E) loops were obtained with a maximum electric field in the range 30–50 kV cm^{-1}. At lower field levels, elliptical P-E loops were processed to derive the field-dependent real and imaginary parts of the relative permittivity, ε_r' and ε_r'' [17].

3. Results and discussion

X-ray powder diffraction patterns of crushed, sintered pellets were indexed on the basis of a Pb4m Space Group, as adopted by Graetsch [7] (ICCD 05–001–0283). For undoped CBN28, calcined at 1200 ºC for 4 h then sintered, orthorhombic $CaNb_2O_6$ secondary phase was detected (ICCD 00–011–0619), indicating incomplete reaction of precursors. Other secondary phase peaks were present in w = 0.05 (Fig. 2), suggesting that this doping level may be beyond the solid solution limits; these included $CaNb_2O_6$, a tetragonal $Ba_3Nb_5O_6$ (ICCD 00–031–0158), and cubic Ba-Y-Niobate or Ba-Ca-Y-Niobate

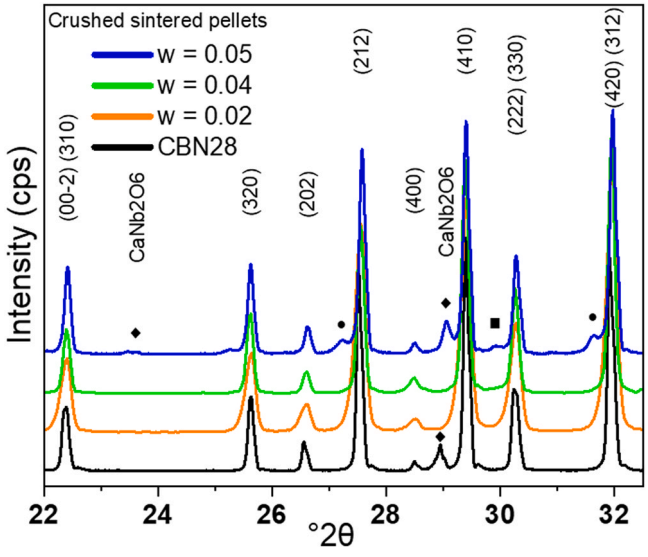

Fig. 2. X-ray diffraction patterns of $(Ca_{0.28}Ba_{0.72})_{1-3w/2}Y_wNb_2O_6$ [0 ≤ w ≤ 0.05], indexed according to P4bm, ICCD 05–001–0283. Symbol ◆ represents orthorhombic $CaNb_2O_6$ (ICCD 00–011–0619); • represents tetragonal $Ba_3Nb_5O_6$ (ICCD 00–031–0158); ■ corresponds to a 100% R.I. peak in a cubic structure whose composition is either Ba_2YNbO_6 (ICCD 00–024–1042) or $Ba_2Ca_{0.79}Nb_{1.08}O_{5.68}Y_{0.13}$ (ICCD 04–021–7855).

phases (ICCD 00–024–1042 and ICCD 04–021–7855). Lattice parameters of the CBN28 phase resulting from Rietveld refinement, Fig. 3, are presented in Table 1. There was a slight contraction in the *c* lattice parameter with increasing Y content, consistent with solid solution formation and the substitution of the smaller Y^{3+} ion for Ca^{2+}/Ba^{2+}, as intended.

The experimentally measured densities of the sintered samples were 5.11–5.18 g/cm^3 for compositions w = 0 (CBN28) to w = 0.04, Table 2. Relative density was 4.96 g/cm^3 (94%) for w = 0.05. Secondary electron micrographs of $(Ca_{0.28}Ba_{0.72})_{1-3w/2}Y_wNb_2O_6$ [0 ≤ w ≤ 0.05] are shown in Fig. 3. Apparent high porosity in CBN28, Fig. 3(a), may in part be caused by grain pull-out, given its higher measured density, when compared with similarly porous w = 0.05 Fig. 3(d).

Fig. 4 shows similar grain sizes for different dopant levels ≤ 8 µm, except for w= 0.04 where grains are up to ~12 µm in size. Reasons for these observations are thought to relate to different sintering conditions and the presence of secondary phase in some samples. It had been found that for CBN28 and w = 0.02 the highest densities could be obtained by two-step sintering at 1350 °C and 1200 °C, whereas for w = 0.04 and 0.05 optimum densities were achieved by processing at 1325 °C and 1250 °C. The increased grain growth in w = 0.04 may be due to these differences in thermal processing. For sample composition w = 0.05 which underwent the same sintering conditions as w = 0.04, the presence of secondary phases (absent in w = 0.04, Table 1) may have inhibited grain growth thereby offsetting any thermal effect. Columnar grains, which are common in TBs due to a preferential [001] growth habit, were not observed. Microcracking was evident by SEM in undoped CBN, this phenomenon was less evident in w = 0.04 and absent in w = 0.05, Fig. 4.

Plots of relative permittivity versus temperature are shown in Fig. 5. The relative permittivity of the undoped CBN28 ceramic showed a peak value of 2086 at a temperature of 268 °C, with no evidence of frequency dispersion (relaxor behaviour) between 1 kHz and 1 MHz. The substitution of Y^{3+} up to w = 0.02 caused a significant reduction in the temperature of the permittivity maxima to 188 °C, with some evidence of frequency dependency of permittivity now appearing. The change in response between CBN28 and w = 0.02 provides further evidence that Y ions had been incorporated into the tungsten bronze structure and these, plus the corresponding A-site vacancies, acted to destabilise the ferroelectric phase. On increasing the level of Y substitution to w = 0.04 there was a change to a very broad permittivity peak with more significant frequency dependence, consistent with weak relaxor behaviour. The temperature of the permittivity maximum, T_m, was 146 °C at 1 kHz increasing to 152 °C at 1 MHz. Variation of permittivity for w = 0.04 remained within ± 15% of the median value (ε_r =1140) over the temperature range from 71 to 210 ºC, when measured at 1 kHz. For w = 0.05, the permittivity maximum temperature, T_m, was slightly more sensitive to measurement frequency, with T_m occurring at 141 °C and 150 °C, when measured at 1 kHz and 1 MHz respectively. Temperature stability of permittivity was also further improved, remaining within ± 15% of the median value (ε_r = 910) from 36° to 218°C.

Dielectric loss tangent, tan δ, values were ≤ 0.1 for frequencies of 1 kHz for the temperature range investigated (−70 to 350 ºC) for samples CBN28 and w= 0.05. For w = 0.02 and w = 0.04, measured at frequencies of 1 kHz and 10 kHz, the tan δ values increased sharply above a temperature of ~250 °C. A future detailed study of loss mechanisms would provide a foundation for addressing the relatively high losses.

The polarisation-electric field (P-E) responses showed a negligible change in character between CBN28 and Y^{3+} inclusion up to dopant level w = 0.02 (Fig. 6a). The coercive field strength (E_c) and remnant polarisation (P_r) values were determined as 14.2 kV cm^{-1} and 2.4 µC/cm^2 respectively for the undoped CBN28 (E_{max} = 30 kV cm^{-1}). Equivalent values for w = 0.02 were 13.9 kV cm^{-1} and 2.3 µC/

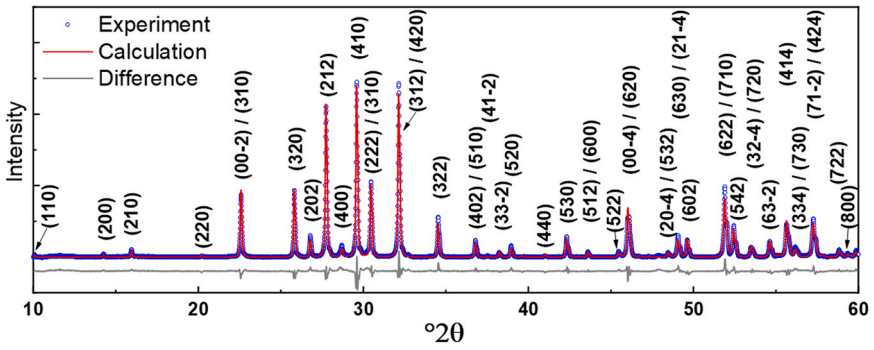

Fig. 3. Full pattern Rietveld refinement for $(Ca_{0.28}Ba_{0.72})_{1-3w/2}Y_wNb_2O_6$ [w = 0.04], indexed according to P4bm, ICCD 05–001–0283.

Table 1
Summary of (pseudo) tetragonal lattice parameters from the refinement of $(Ca_{0.28}Ba_{0.72})_{1-3w/2}Y_wNb_2O_6$ [$0 \le w \le 0.05$] indexed to space group P4bm. The R_{wp} 'goodness of fit' values, calculated theoretical density (ρ) and estimated percentage of $CaNb_2O_6$ secondary phase are also listed.

Sample Code	a (Å)	c (Å)	Volume (Å^3)	R_{wp} (%)	Theoretical ρ (g/cm^3)	$CaNb_2O_6$ (wt%)
CBN28	12.4574 (2)	7.8976 (1)	1225.52 (2)	9.81	5.31	5.3
w = 0.02	12.4538(1)	7.8901(1)	1223.74 (1)	9.85	5.30	-
w = 0.04	12.4555(1)	7.8881 (2)	1223.75 (3)	9.93	5.28	-
w = 0.05	12.4589 (2)	7.8762 (7)	1222.52 (2)	10.06	5.27	6.7

Table 2
Summary of experimentally measured density data.

Sample Code	Nominal formula	ρ (g/cm^3)	Density (%)
CBN28	$Ca_{0.28}Ba_{0.72}Nb_2O_6$	5.11	96.2
w = 0.02	$(Ca_{0.28}Ba_{0.72})_{0.97}Y_{0.02}Nb_2O_6$	5.18	97.8
w = 0.04	$(Ca_{0.28}Ba_{0.72})_{0.94}Y_{0.04}Nb_2O_6$	5.14	97.3
w = 0.05	$(Ca_{0.28}Ba_{0.72})_{0.925}Y_{0.05}Nb_2O_6$	4.96	94.1

cm^2. However, the P-E response changed significantly for the higher Y^{3+} contents, w = 0.04 and w = 0.05, each of which had displayed evidence of relaxor behaviour in their permittivity-temperature plots (Fig. 5). The P_r values consequently decreased to 1.5 μC/cm^2 for w = 0.04 and 0.8 μC/cm^2 for w = 0.05. The coercive field values decreased to 8.2 kV cm^{-1} for w = 0.04 and 5.1 kV cm^{-1} for w = 0.05. The narrower ferroelectric loops (lower E_c values) for w = 0.04 and w = 0.05, are consistent with a reduction in polar length scales, giving a lower energy barrier for 'domain' reorientation relative to ferroelectric samples (CBN28 and w = 0.02) (Table 3).

At sub-coercive field levels, for example 5 kV cm^{-1}, Fig. 6(b) the P-E loops for each composition, exhibited an elliptical form, similar to those reported previously in conventional perovskite-type ferroelectrics [17]. At these field levels the domain structures of the

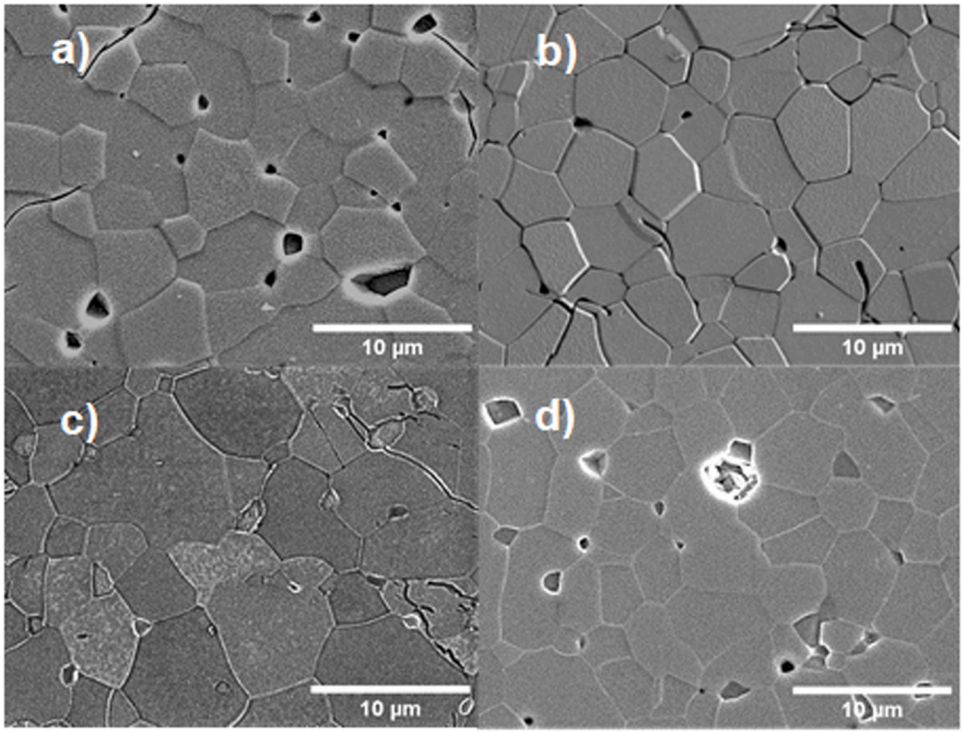

Fig. 4. SEM secondary electron micrographs of $(Ca_{0.28}Ba_{0.72})_{1-3w/2}Y_wNb_2O_6$ [$0 \le w \le 0.05$]: a) CBN28, b) w = 0.02 c) w= 0.04 d) w = 0.05.

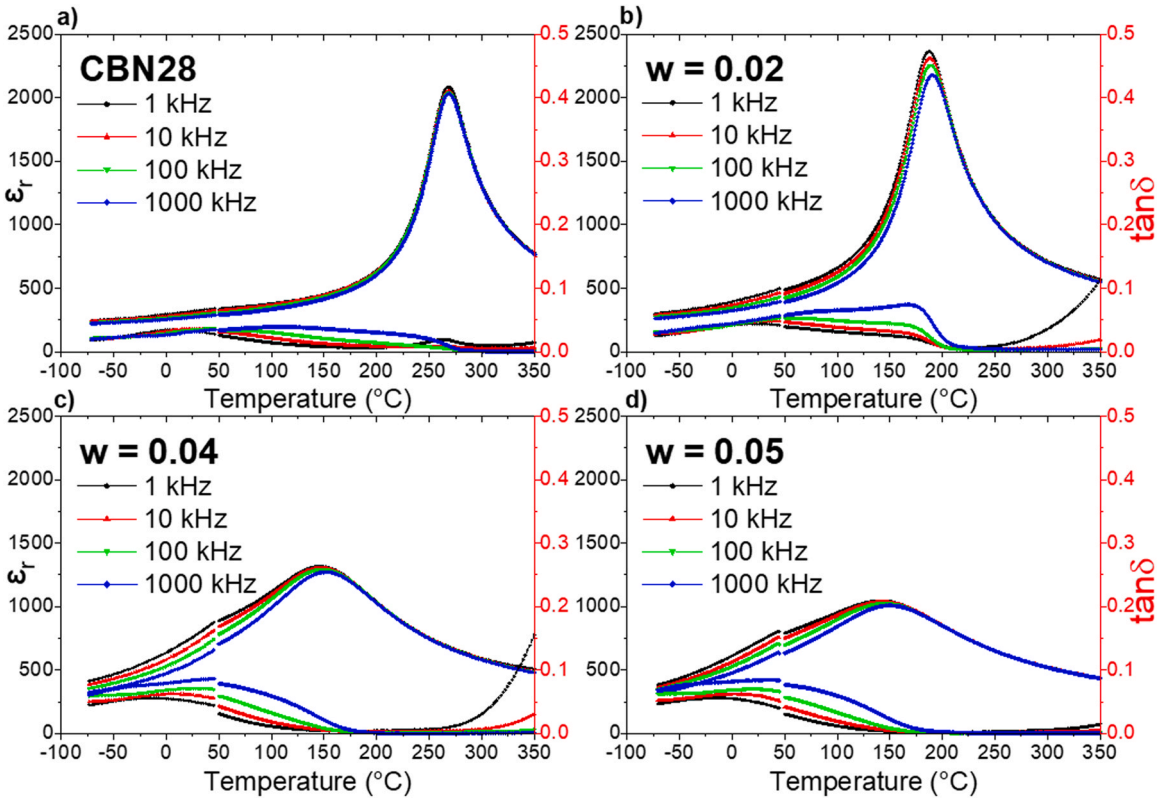

Fig. 5. Relative permittivity-temperature and loss tangent–temperature responses for $(Ca_{0.28}Ba_{0.72})_{1-3w/2}Y_wNb_2O_6$ [$0 \le w \le 0.05$] ceramics, measured at a 1–1000 kHz. a) CBN28, b) w= 0.02c) w = 0.04, d) w = 0.05.

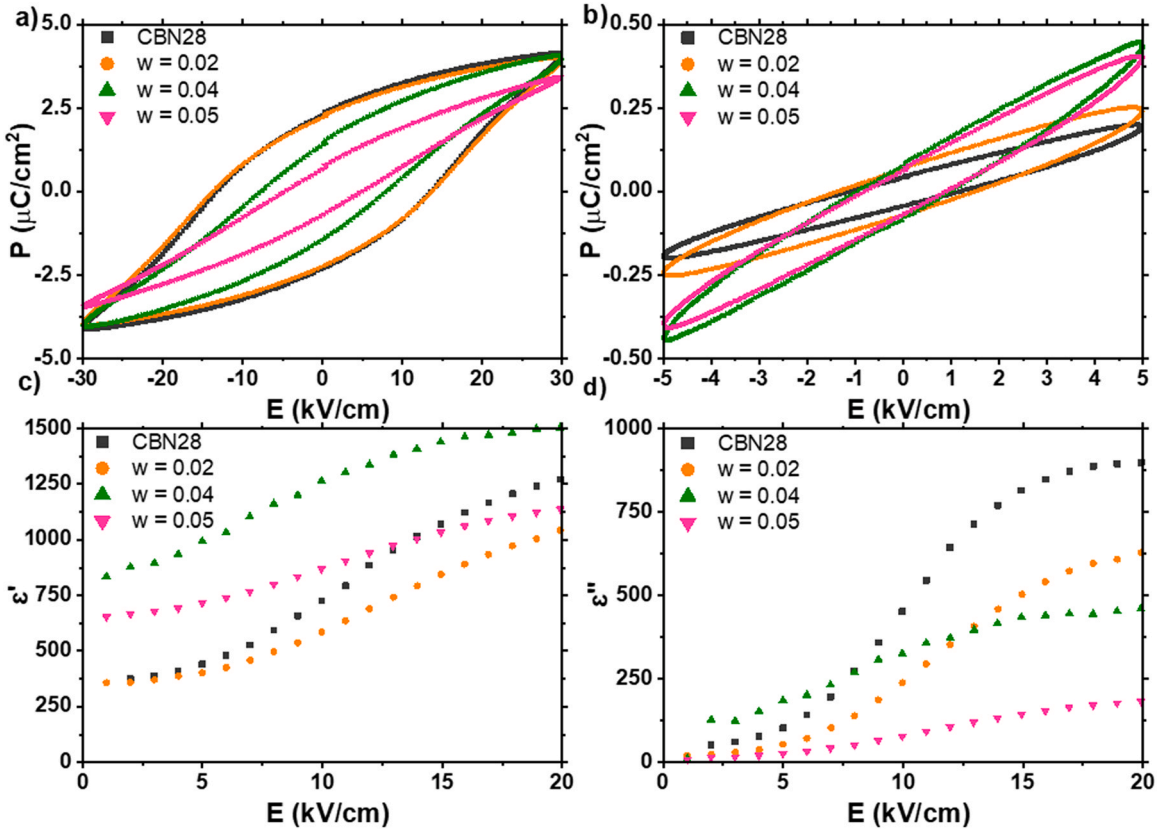

Fig. 6. Comparison of P-E loops for $(Ca_{0.28}Ba_{0.72})_{1-3w/2}Y_wNb_2O_6$ [$0 \le w \le 0.05$] ceramics at a) 30 $kVcm^{-1}$ and b) 5 $kVcm^{-1}$ and variation in (c) real and (d) imaginary parts of the permittivity as a function of electric-field amplitude.

Table 3
Summary of dielectric data for $(Ca_{0.28}Ba_{0.72})_{1-3w/2}Y_wNb_2O_6$ [$0 \le w \le 0.05$] ceramics, permittivity values measured at 1 kHz unless otherwise stated. Maximum polarisation (P_{max}), residual polarisation (P_r) and coercive field (E_c) were measured under a maximum applied field of (+)30 kV cm^{-1}.

Sample Code	Nominal formula	T_m @ 1 kHz (°C)	T_m @ 1 MHz (°C)	ε_r max	$\Delta\varepsilon_r$ FWHM (°C)	P_{max} (μC cm^{-2})	P_r (μC cm^{-2})	E_c (kV cm^{-1})
CBN28	$Ca_{0.28}Ba_{0.72}Nb_2O_6$	268	269	2086	71	4.1	2.4	14.2
w = 0.02	$(Ca_{0.28}Ba_{0.72})_{0.97}Y_{0.02}Nb_2O_6$	188	191	2364	73	4.0	2.3	13.9
w = 0.04	$(Ca_{0.28}Ba_{0.72})_{0.94}Y_{0.04}Nb_2O_6$	146	152	1315	183	4.0	1.5	8.2
w = 0.05	$(Ca_{0.28}Ba_{0.72})_{0.925}Y_{0.05}Nb_2O_6$	141	150	1043	181	3.4	0.8	5.1

samples were not sufficiently re-ordered or "poled", by the applied field, and so lower residual polarisations were recorded in comparison to the P-E loops acquired at the higher applied fields The gradients of the P-E loops for w = 0.04 and w = 0.05 were significantly higher than those for CBN28 and w = 0.02, consistent with the higher dielectric permittivity values of the former in the range close to room temperature. The P-E data were subsequently processed further to yield field-dependent values for the complex dielectric permittivity, with the real part ($\varepsilon_r^{/}$) corresponding approximately to the gradient and the imaginary part ($\varepsilon_r^{//}$) to the area (hysteresis loss) enclosed within the loop [17].

Both the $\varepsilon_r^{/}$-E_0 and $\varepsilon_r^{//}$-E_0 relationships exhibited a relatively field-independent region at low electric field amplitudes, followed by a near-linear region (the Rayleigh region) and eventually a tendency towards saturation at high fields, Fig. 6(c-d). These characteristics are also similar to those observed in the more common perovskite-structured ferroelectrics [18]. The Rayleigh coefficients, $\alpha^{/}$ and $\alpha^{//}$, were determined as the gradients of the $\varepsilon_r^{/}$-E_0 and $\varepsilon_r^{//}$-E_0 relationships in the electric field range between 5 and 15 kV cm^{-1}. These values, summarised in Table 4, demonstrate a gradual reduction in the field-dependent, extrinsic ferroelectric domain wall contributions to dielectric permittivity and loss with increasing substitution of Y^{3+} in solid solution. The $\alpha^{/}$ values for CBN28 and w = 0.05 were determined as 0.67×10^{-3} and 0.33×10^{-3} m V^{-1} respectively, which are significantly lower than those reported for typical soft lead zirconate titanate (PZT) ceramics (5.3×10^{-3} m V^{-1}) but comparable with that of hard PZT (0.83×10^{-3} m V^{-1}) [18]. Modification of the Rayleigh coefficients provides further evidence for the disruption of ferroelectric ordering and changes to polarisation dynamics in Y-doped CBN28.

There are limited reports of the effects of other CBN dopants. CBN28 was singly doped by the addition of CeO_2 or La_2O_3 prior to sintering, at $0 \le$ wt% ≤ 0.6. For both the Ce and La doped compositions, with a dopant wt% of 0.5, broadening of the ε_r-T was observed, greater than that seen in the present work's w = 0.02 (0.455 wt% Y), where $\varepsilon_r = 2055 \pm 15\%$ from 166 to 211 °C, but less than w = 0.04 ($\varepsilon_r = 1143 \pm 15\%$ from 71 to 210 °C) and 0.05 ($\varepsilon_r = 908 \pm 15\%$ from 37 to 218°C). Based on the published ε_r-T plots the estimated temperature range of ± 15% stability was from approximately 160 to 223 °C for CBN-0.5 wt%CeO_2 and 152–212 °C for CBN-0.5 wt%La_2O_3 [19]. The temperature of the permittivity peak, T_m, decreased to 190 °C for both CBN-0.5 wt%CeO_2 and CBN-0.5 wt%La_2O_3, when measured at 10 kHz [19]. Here we record a similar reduction in T_m with low level Y inclusion up to w = 0.02, to 188 °C.

Other reports show the effects of Na^+ substitution according to the general formula $(Ca_{0.28}Ba_{0.72})_{2.5-0.5x}Na_xNb_5O_{15}$ [$0 \le x \le 1$] [20]. In the composition x = 0.8 the temperature of the permittivity maxima increased to 332 °C and there was a negligible effect on the breadth of the permittivity temperature response. Subsequent B-site substitution of Nb^{5+}, by Sb^{5+} or Ta^{5+}, in the (x = 0.8) Na- doped CBN decreased T_m but also increased the level of ε_r-T peak broadening, most notably for Sb-modified compositions. For example, the composition $(Ca_{0.28}Ba_{0.72})_{2.1}Na_{0.8}Nb_4Ta_1O_{15}$, where $\varepsilon_r = \sim 820 \pm 15\%$ from ~−90 to ~180 °C, when measured at 10 kHz [21].

Table 4
Rayleigh coefficients of Y-doped CBN ceramics obtained from nonlinear field-dependent dielectric properties.

Sample Code	Nominal formula	$\alpha^{/}$ (10^{-3} m V^{-1})	$\alpha^{//}$ (10^{-3} m V^{-1})
CBN28	$Ca_{0.28}Ba_{0.72}Nb_2O_6$	0.67	0.78
w = 0.02	$(Ca_{0.28}Ba_{0.72})_{0.97}Y_{0.02}Nb_2O_6$	0.46	0.48
w = 0.04	$(Ca_{0.28}Ba_{0.72})_{0.94}Y_{0.04}Nb_2O_6$	0.46	0.26
w = 0.05	$(Ca_{0.28}Ba_{0.72})_{0.925}Y_{0.05}Nb_2O_6$	0.33	0.12

4. Conclusion

Yttrium doped $Ca_{0.28}Ba_{0.72}Nb_2O_6$ ceramics of the tungsten bronze structure were prepared by the solid-state method. A transition from ferroelectric to relaxor type behaviour of CBN28 was induced by Y-doping at levels of w = 0.04 and w = 0.05 in the ceramic formulation $(Ca_{0.28}Ba_{0.72})_{1-3w/2}Y_wNb_2O_6$ [$0 \le w \le 0.05$]. This assumed Y^{3+} substitution and vacancy inclusion on A-sites of the tungsten bronze structure resulted in a diffuse permittivity-temperature peak. Results suggest that further research into doped $Ca_{0.28}Ba_{0.72}Nb_2O_6$ holds potential for achieving new high temperature dielectrics, particularly if a strategy for decreasing dielectric loss values can be developed.

CRediT authorship contribution statement

Harry Peirson: Data curation, Investigation, Formal analysis, Methodology, Writing – original draft. **Juncheng Pan:** Data curation, Investigation, Formal analysis. **Yizhe Li:** Data curation, Investigation, Formal analysis. **David A. Hall:** Formal analysis, Methodology. **Andy P. Brown:** Writing – review & editing. **Rik M. Drummond-Brydson:** Writing – review & editing. **Steven J. Milne:** Writing – review & editing, Conceptualization.

Data availability

Data will be made available on request.

Declaration of Competing Interest

The authors declare the following financial interests/personal relationships which may be considered as potential competing interests: Steven J. Milne reports financial support was provided by UK Research Council. David A. Hall reports financial support was provided by Engineering and Physical Sciences Research Council. David A. Hall reports financial support was provided by UK Research Council.

Acknowledgements

This work was performed as part of projects funded by the UK Research Council at Leeds and Manchester: award numbers EP/S029036/1 and EP/S028978/1 respectively. Funding was also provided by the Engineering and Physical Sciences Research Council: award numbers EP/S028978/1 and EP/V053183/1. A Ph.D. scholarship for H. Peirson was provided by School of Chemical and Process Engineering, University of Leeds.

References

[1] P.G. Dickens, M.S. Whittingham, The tungsten bronzes and related compounds, Q. Rev. Chem. Soc. 22 (1968) 30–44, https://doi.org/10.1039/QR9682200030

[2] R.R. Neurgaonkar, J.R. Oliver, L.E. Cross, Ferroelectric properties of tetragonal tungsten bronze single crystals, Ferroelectrics 56 (1984) 31–36, https://doi.org/10.1080/00150198408012713

[3] T. Brown, A.P. Brown, D.A. Hall, T.E. Hooper, Y. Li, S. Micklethwaite, Z. Aslam, S.J. Milne, New high temperature dielectrics: Bi-free tungsten bronze ceramics with stable permittivity over a very wide temperature range, J. Eur. Ceram. Soc. 41 (2021) 3416–3424, https://doi.org/10.1016/j.jeurceramsoc.2020.10.034

[4] L. Cao, Y. Yuan, X. Meng, E. Li, B. Tang, Ferroelectric-relaxor crossover and energy storage properties in $Sr_2NaNb_5O_{15}$-based tungsten bronze ceramics, ACS Appl. Mater. Interfaces 14 (2022) 9318–9329, https://doi.org/10.1021/acsami.1c23673

[5] S. Ke, H. Fan, H. Huang, H.L.W. Chan, S. Yu, Dielectric, ferroelectric properties, and grain growth of $Ca_xBa_{1-x}Nb_2O_6$ ceramics with tungsten bronzes structure, J. Appl. Phys. 104 (2008) 024101, https://doi.org/10.1063/1.2956615

[6] C.J. Lu, Y.J. Qi, Incommensurate modulation structure in ferroelectric $Ca_{0.28}Ba_{0.72}Nb_2O_6$ single crystals of tungsten bronze structure, Appl. Phys. Lett. 89 (2006) 191901, https://doi.org/10.1063/1.2364840

[7] H.A. Graetsch, C.S. Pandey, J. Schreuer, M. Burianek, M. Mühlberg, Incommensurate modulation of calcium barium niobate (CBN28 and Ce:CBN28), Acta Crystallogr. B 68 (2012) 101–106, https://doi.org/10.1107/S0108768111054863

[8] M. Muehlberg, M. Burianek, B. Joschko, D. Klimm, A. Danilewsky, M. Gelissen, L. Bayarjargal, G.P. Görler, B.O. Hildmann, Phase equilibria, crystal growth and characterization of the novel ferroelectric tungsten bronzes $Ca_xBa_{1-x}Nb_2O_6$ (CBN) and $Ca_xSr_yBa_{1-x-y}Nb_2O_6$ (CSBN), J. Cryst. Growth 310 (2008) 2288–2294, https://doi.org/10.1016/j.jcrysgro.2007.12.023

[9] H.A. Graetsch, J. Schreuer, M. Burianek, M. Mühlberg, Thermally induced structural changes in incommensurate calcium barium niobate $Ca_{0.28}Ba_{0.72}Nb_2O_6$ (CBN28), J. Solid State Chem. 196 (2012) 255–266, https://doi.org/10.1016/j.jssc.2012.06.028

[10] C.S. Pandey, J. Schreuer, M. Burianek, M. Mühlberg, Relaxor behavior of $Ca_xBa_{1-x}Nb_2O_6$ ($0.18 \le x \le 0.35$) tuned by Ca/Ba ratio and investigated by resonant ultrasound spectroscopy, Phys. Rev. B 87 (2013) 094101, https://doi.org/10.1103/PhysRevB.87.094101

[11] F. Hu, X. Chen, P. Peng, F. Cao, X. Dong, G. Wang, High permittivity $(1-x)Bi_{1/2}Na_{1/2}TiO_3$-$xPbMg_{1/3}Nb_{2/3}O_3$ ceramics for high-temperature-stable capacitors, J. Am. Ceram. Soc. 101 (2018) 4434–4440, https://doi.org/10.1111/jace.15730

[12] N. Kumari, S. Monga, M. Arif, N. Sharma, A. Singh, V. Gupta, P.M. Vilarinho, K. Sreenivas, R.S. Katiyar, Higher permittivity of Ni-doped lead zirconate titanate, $Pb[(Zr_{0.52}Ti_{0.48})_{(1-x)}\ Ni_x]O_3$, ceramics, Ceram. Int. 45 (2019) 4398–4407, https://doi.org/10.1016/j.ceramint.2018.11.117

[13] A. Zeb, S.J. Milne, High temperature dielectric ceramics: a review of temperature-stable high-permittivity perovskites, J. Mater. Sci. Mater. Electron. 26 (2015) 9243–9255, https://doi.org/10.1007/s10854-015-3707-7

[14] A. Zeb, Y. Bai, T. Button, S.J. Milne, Temperature-stable relative permittivity from −70°C to 500°C in $(Ba_{0.8}Ca_{0.2})TiO_3$–$Bi(Mg_{0.5}Ti_{0.5})O_3$–$NaNbO_3$ ceramics, J. Am. Ceram. Soc. 97 (2014) 2479–2483, https://doi.org/10.1111/jace.12949

[15] D.-S. Tang, J.-K. Liang, T.-J. Shi, Y.-L. Zhang, J.-H. Tian, W.-X. Li, Investigation of the pseudo-ternary system $SrNb_2O_6$-$NaNbO_3$-$LiNbO_3$, Acta Phys. Sin. 28 (1979) 62–77, https://doi.org/10.7498/aps.28.62

[16] M. Stewart, M.G. Cain, D.A. Hall, Ferroelectric Hysteresis Measurement and Analysis, National Physical Laboratory, Teddington, UK. CMMT(A), 1999, pp. 1–57 ⟨http://eprintspublications.npl.co.uk/id/eprint/1118⟩.

[17] D.A. Hall, M.M. Ben-Omran, P.J. Stevenson, Field and temperature dependence of dielectric properties in $BaTiO_3$-based piezoceramics, J. Phys. Condens. Matter 10 (1998) 461–476, https://doi.org/10.1088/0953-8984/10/2/025

[18] D.A. Hall, P.J. Stephenson, High field dielectric behaviour of ferroelectric ceramics, Ferroelectrics 228 (1999) 139–158, https://doi.org/10.1080/00150199908226132

[19] L. Wei, Z. Yang, X. Chao, H. Jiao, Structure and electrical properties of $Ca_{0.28}Ba_{0.72}Nb_2O_6$ ceramics with addition of rare earth oxides (CeO_2, La_2O_3), Ceram. Int. 40 (2014) 5447–5453, https://doi.org/10.1016/j.ceramint.2013.10.130

[20] B. Yang, L. Wei, X. Chao, Z. Wang, Z. Yang, Role of structural modulation in electrical properties of tungsten bronze $(Ca_{0.28}Ba_{0.72})_{2.5-0.5x}Na_xNb_5O_{15}$ ceramics, J. Alloy. Compd. 632 (2015) 368–375, https://doi.org/10.1016/j.jallcom.2015.01.247

[21] B. Yang, S. Hao, P. Yang, L. Wei, Z. Yang, Relaxor behavior and energy storage density induced by B-sites substitutions in $(Ca_{0.28}Ba_{0.72})_{2.1}Na_{0.8}Nb_5O_{15}$ tungsten bronze ceramics, Ceram. Int. 44 (2018) 8832–8841, https://doi.org/10.1016/j.ceramint.2018.02.065